Applied Surface Science 636 (2023) 157780

Contents lists available at ScienceDirect

Applied Surface Science

journal homepage: www.elsevier.com/locate/apsusc

Full Length Article

Deterioration of the 2G HTS tapes by the Ne^+ ions irradiation (250 keV)

Paweł Pęczkowski [a,*], Ryszard Zalecki [b], Piotr Zachariasz [c], Elżbieta Szostak [d], Jarosław Piętosa [e], Marcin Turek [f], Krzysztof Pyszniak [f], Marcin Zając [g], Joanna Czub [b], Łukasz Gondek [b]

[a] Institute of Physical Sciences, Faculty of Mathematics and Natural Sciences, School of Exact Sciences, Cardinal Stefan Wyszyński University, K. Wóycickiego 1/3 Street, 01-938 Warsaw, Poland
[b] Department of Solid State Physics, Faculty of Physics and Applied Computer Science, AGH University of Science and Technology, Mickiewicza 30 Avenue, 30-059 Kraków, Poland
[c] Center for Functional Materials, Łukasiewicz Research Network – Institute of Microelectronics and Photonics, Zabłocie 39 Street, 30-701 Kraków, Poland
[d] Faculty of Chemistry, Jagiellonian University, Gronostajowa 2 Street, 30-387 Kraków, Poland
[e] Group of Phase Transition, Division of Physics of Magnetism, Institute of Physics, Polish Academy of Sciences, Lotników 32/46 Avenue, 02-668 Warsaw, Poland
[f] Institute of Physics, Maria Curie Skłodowska University, pl. M. Curie-Skłodowskiej 1, 20-031 Lublin, Poland
[g] National Synchrotron Radiation Centre SOLARIS, Jagiellonian University, Czerwone Maki 98 Street, 30-392 Kraków, Poland

ARTICLE INFO

Keywords:
2G HTS superconducting tapes
Ne^+ ion irradiation
X-ray diffraction
X-ray absorption spectroscopy
Radiation damage

ABSTRACT

We discuss changes in properties of Gd-based high-temperature superconducting (HTS) tapes induced by 250 keV Ne^+ ions irradiation. HTS tapes are used in devices operating in extreme radiation conditions with the prospect of using them in space industry. Ionizing radiation, including heavy ion bombardment, can introduce defects (e.g. Schottky, Frenkel ones) to the microstructure of tapes, leading to deterioration of the superconducting parameters. Therefore, the superconducting layer of the tape was implanted with fluences from 10^{12} to 10^{14} Ne^+/cm^2 to determine the cosmic ray irradiation effect. Comprehensive studies of the microstructural, structural, magnetic, and electrical properties of the irradiated tapes prove the microscopic origin of their deterioration. It is mainly due to oxygen deficiency and microstructural as well as structural defects. The critical current densities are reduced by 33% – 60% (depending on the external magnetic field) compared to the reference sample.

1. Introduction

The widespread application of high-temperature superconducting (HTS) materials is currently at a watershed moment. Recently, there has been a growing interest in new superconductors with higher parameters, such as critical current and critical temperature, with lower production costs, which is crucial from the applicability point of view [1]. Prior to the discovery of HTS by Bednorz and Müller in the La–Ba–Cu–O, which historically was the first HTS superconductor with a critical temperature (T_c) close to 36 K, in the pioneering phase of superconductivity research, the practical application of the type-II superconductors was already envisioned by Geballe and Hulm [2,3]. Later, by applying hydrostatic pressure, Chu et al. [4] increased the superconducting critical temperature of the $La_{5-x}Ba_xCu_5O_{5(3-y)}$ up to 50 K, showing experimentally how various parameters can affect T_c. Substituting La with Y atoms or other lanthanides (e.g., Eu, Gd, Dy), the critical temperature was successfully increased to around 90 K [5–8].

The development of superconducting materials, among others HTS tapes, enables a wide range of applications such as motors [9,10], generators [11–13], transformers [14,15], cables [16,17], high field magnets [18], accelerator magnets [19], and new generation superconducting tapes [20]. Such HTS tapes enable the flow of high-intensity electric current without the disadvantageous phenomenon of power dissipation. The second generation (2G) high-temperature superconductor (HTS) tapes in a superconducting state at the temperature of liquid nitrogen (77 K) can conduct an electric current of about 300 A in the self field. Superpower 2G HTS tape with an HTS layer thickness of 0.7 μm (tape thickness of 55 – 65 μm) and a width of 12 mm and an average critical current at 77 K in the self-field is approx. 300 A / 12 mm [21]. During the operation of superconducting devices, 2G HTS tapes are exposed to ionizing radiation and the formation of radiation defects. The above process leads to the gradual degradation of structural and critical parameters of the 2G HTS tapes. It has been shown that the critical current is more sensitive to radiation defects than the critical temperature [19].

2G HTS tapes can be used to construction ion motors or magnetic

* Corresponding author.
E-mail addresses: p.peczkowski@wp.pl, p.peczkowski@uksw.edu.pl (P. Pęczkowski).

https://doi.org/10.1016/j.apsusc.2023.157780
Received 17 March 2023; Received in revised form 26 May 2023; Accepted 12 June 2023
Available online 20 June 2023

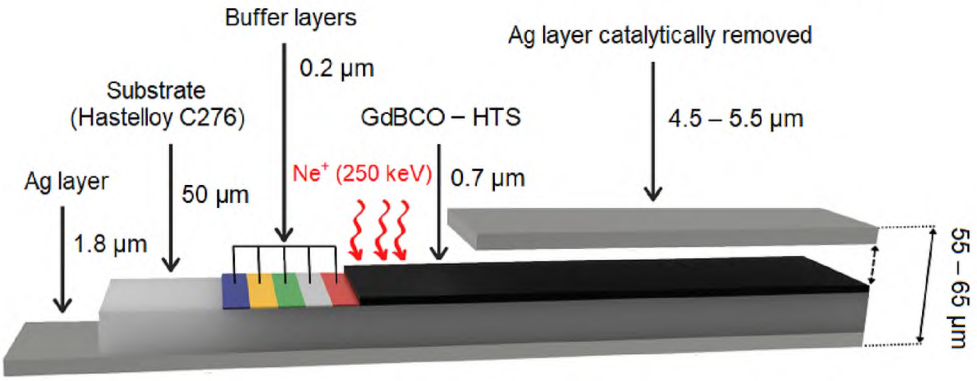

Fig. 1. The cross-section of the 2G HTS SF 12050 superconducting tape by SuperPower Inc. [52,53]. The superconducting GdBCO layer was irradiated with the Ne^+ ions after the Ag layer removal.

screens, e.g. protecting a spacecraft crew against cosmic radiation [22] due to the small dimensions and weight. However, the mechanism of high-energy radiation propagation and induced defects in the 2G HTS superconducting materials has not been sufficiently researched at the fundamental level and requires further theoretical and experimental studies.

As well known, high-energy ions in the solar wind could generate structural and microstructural defects in superconductors, leading, e.g., to eddy currents and superconductivity deterioration. Therefore, it should be emphasized that the proposed topic is a starting point for research of the space industry development and for the other innovative solutions that could potentially be exploited in future space missions operating in a high-energy radiation environment. Furthermore, the proposed topic could also stimulate the invention of new modules of software describing radiation propagation through a superconducting system (Geant4 [23], Fluka [24]).

Exposure to radiation remains one of the most challenging problems for long-term human space exploration missions, including voyages to Mars [25]. The risks associated with long-term exposure to Galactic Cosmic Rays (GCR) [26] and acute exposure to Solar Wind Particle (SPE) events are one of the most critical barriers to planning interplanetary voyages in a crewed spacecraft [27]. The corpuscular part of the radiation consists mainly of protons (90% of particles), α particles (9%), electrons (about 1%), and a few heavier nuclei. The changes in transport properties of 2G HTS tapes under irradiation of neutrons [28–30], protons [31–33], He ions [34–36], heavy ions as oxygen [37,38], or noble gas ions (Ar, Kr, and Xe) [39,40] have been studied [39–42]. In contrast, changes in superconductivity under Ne ions irradiation have not yet been investigated.

Recently, a new method to increase the critical current of these coated tapes at high magnetic fields with ionic irradiation was shown [43]. The proton implantation with an energy of 4 MeV and fluence of $8{\cdot}10^{16}$ protons/cm^2 twice increased the critical currents for $H = 6$ kOe at $T = 27$ K [43]. Further reports confirmed that the critical current enhances due to proton implantation [44–46]. Since protons are light particles, their influence on superconductors differs from that of heavier ions. In a solid state, the free path of protons is one order of magnitude greater than that of heavy ions. As a result, columnar defects, so-called pinning centres, are not generated by protons.

Further studies showed that oxygen ions with an energy irradiation of 3.5 MeV through a protective Ag layer of a 2G HTS superconducting tape could also reproduce the doubling of the critical current density in high magnetic fields [47]. Ag ion implantation can easily create structural defects in a 2G HTS tape, which are highly uniform along the tape length [48]. The controlled implantation can elucidate vortex dynamics and distribute the ions uniformly in the $REBa_2Cu_3O_{7-\delta}$ (*RE*BCO) layer. It is possible to estimate the size of implantation-inducted defects (e.g., Frenkel defect [49]) which serve as the pinning centres of the Abikosov vortices [50] by using SRIM (Stopping and Range of Ions in Matter) [51,52].

Also, high-speed and heavy ions of $^{132}Xe^{23+}$ with energy from 46 MeV to 167 MeV for implantation of the $YBa_2Cu_3O_{7-\delta}$ (YBCO) 2G HTS were researched [42]. Different morphology ion destruction pathways demonstrate different efficacy as the pinning centres. The highest critical current density (J_c) intensification occurs for the lowest ion energy (46 MeV) in the energy loss range of 8.9 keV/nm – 4.7 keV/nm for the Xe ions. The samples showed the highest J_c of 56.0 MA·cm^{-2} (4.2 K) and 3.0 MA·cm^{-2} (77 K) in the self-field, while in a magnetic field of 80 kOe values of 17.0 MA·cm^{-2} (4.2 K) and 1.6 MA·cm^{-2} (77 K) [39]. Similarly, increased J_c, improved adhesion between the superconducting layer and the substrate, and reduced internal stresses are observed under exposure to low doses of Ar and Kr ions irradiation [39]. The critical temperature (T_c) and the critical current density (J_c) decrease as an irradiation fluence increases. It was evidenced that the superconducting phase disappears for the fluence of $5{\cdot}10^{12}$ for $^{132}Xe^{27+}$ ions/cm^2 and 10^{13} for $^{86}Kr^{17+}$ ions/cm^2 [39]. For protons irradiation of 2.5 MeV, the radiation resistance of the $GdBa_2Cu_3O_{7-\delta}$ (GdBCO) 2G HTS tape is higher than that of the YBCO tapes [39]. Compared to the YBCO tapes, the 2G HTS tape (GdBCO-based) exhibits better irradiation resistance due to the higher density of the GdBCO than the YBCO. The threshold for a decrease of the critical current densities is $6.2{\cdot}10^{15}$ protons/cm^2 for the GdBCO tapes and $2.7{\cdot}10^{15}$ protons/cm^2 for YBCO tapes [39].

This work reports the analysis of the microstructure, structure, superconducting, and magnetic properties of the GdBCO 2G HTS tapes after the Ne^+ ions irradiation. The 2G HTS of the type SF (Stabilizer Free) 12050 superconducting tapes (Fig. 1), manufactured by SuperPower Inc. made using the thin-film technology based on the non-magnetic Hastelloy C276 alloy 50 μm thick substrate, were used for the investigation [52,53] The thickness of the investigated superconducting layer equaled to 0.70 μm (based on the producer data and the SEM investigation). In the original, an Ag film of about 5 μm covered the HTS tape, which was removed for the experiment.

2. Experimental details

2.1. Preparation of the irradiated tapes

The 2G HTS SF 12050 superconducting tapes with the critical current densities (J_c) of 3.7 MA·cm^{-2} at $T = 77$ K, a width of 12 mm, and a thickness of about 55 μm were used. At first, the protective Ag layer was removed in a catalytic process before irradiation of the superconducting material by noble gas ions. Then, irradiation with an energy of 250 keV and with four selected fluences (10^{12}, $5{\cdot}10^{12}$, 10^{13}, 10^{14} Ne^+/cm^2) was performed using the UNIMAS-79 implanter at the Institute of Physics of the Maria Curie-Skłodowska University in Lublin (Poland). An arc discharge ion source produced the Ne^+ ion beam [54,55], extracted

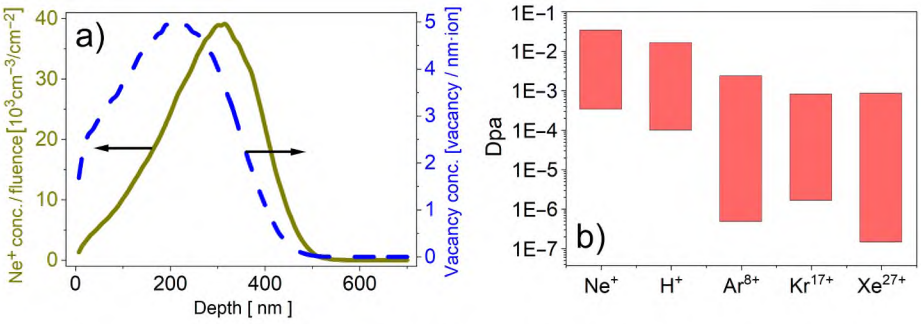

Fig. 2. (**a**) Depth distribution of Ne^+ introduced into the 2G HTS layer (solid line) and depth distribution of vacancies (dashed line) produced during the bombardment; (**b**) Dpa - displacements per atom (logarithmic scale) for Ne^+ and comparison at the same fluences for H^+ [39], and $^{40}Ar^{8+}$ [40], $^{84}Kr^{17+}$ [40], $^{132}Xe^{27+}$ [40], at the same fluences.

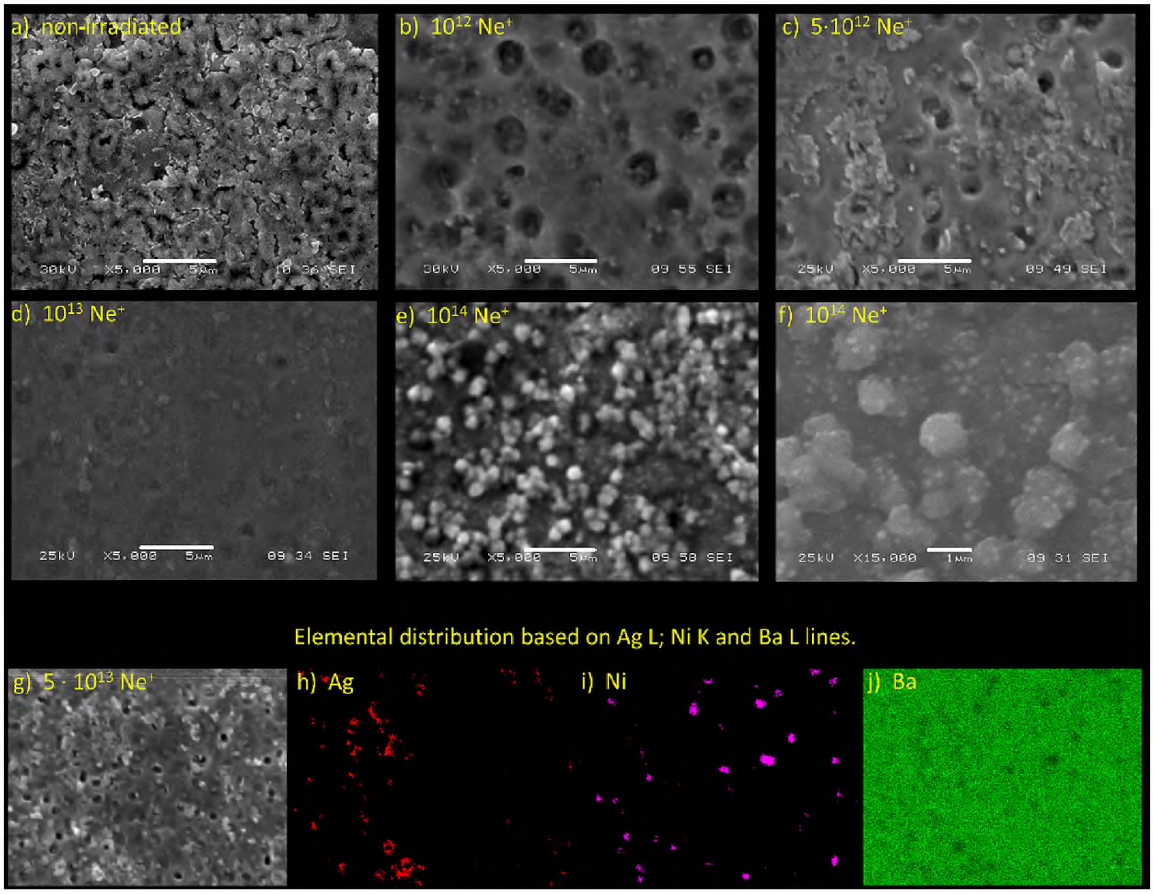

Fig. 3. SEM images of the superconducting layer surfaces for the non-irradiated sample (**a**) and different levels of the Ne^+ irradiation (**b-f**). Elemental distribution maps for the irradiated tape with the fluence of $5{\cdot}10^{12}$ Ne^+/cm^2 (**g-j**).

using 25 kV voltage, then mass-separated using a 90° sector electromagnet and accelerated to 250 keV. In the target chamber was the pressure of 10^{-7} mbar, and irradiation was performed at 298 K. The irradiation current for the two lowest fluences (10^{12} Ne^+/cm^2 and $5{\cdot}10^{12}$ Ne^+/cm^2) was ~20 nA/cm^2 and by order of magnitude larger for the other two fluences (10^{13} Ne^+/cm^2 and 10^{14} Ne^+/cm^2).

Fig. 2a presents the depth distribution of Ne^+ introduced into the 2G HTS layer (solid line) and the depth distribution of vacancies (dashed line) produced during the bombardment. Distributions were calculated using SRIM software [56]. The simulation was performed in the full damage cascade regime, with default SRIM displacement energy values, i.e., 25 eV for Gd, Ba, Cu, and 28 eV for O. As one can see, the depth profile is relatively wide, with mean ion range 270 ± 100 nm. Some parts of Ne^+ ions enter the sample regions lying at a depth of 500 nm. The even wider vacancy distribution profile is shifted towards the 2G HTS layer surface. Nevertheless, the highest possible depth of implantation-induced damage is ~450– 500 nm. The produced damage could be estimated as 0.00034, 0.00170, 0.00340, 0.03400 dpa (displacements per atom) for fluences 10^{12}, $5{\cdot}10^{12}$, 10^{13}, 10^{14} Ne^+/cm^2, respectively [57] (Fig. 2b). In Fig. 2b, apart from Ne^+, displacements per atom with the same fluences for H^+ [39], $^{40}Ar^{8+}$ [40], $^{84}Kr^{17+}$ [40], and $^{132}Xe^{27+}$ [40] are shown for comparison.

2.2. Characterization methods

The microstructure and energy dispersive X-ray spectroscopy (EDS)

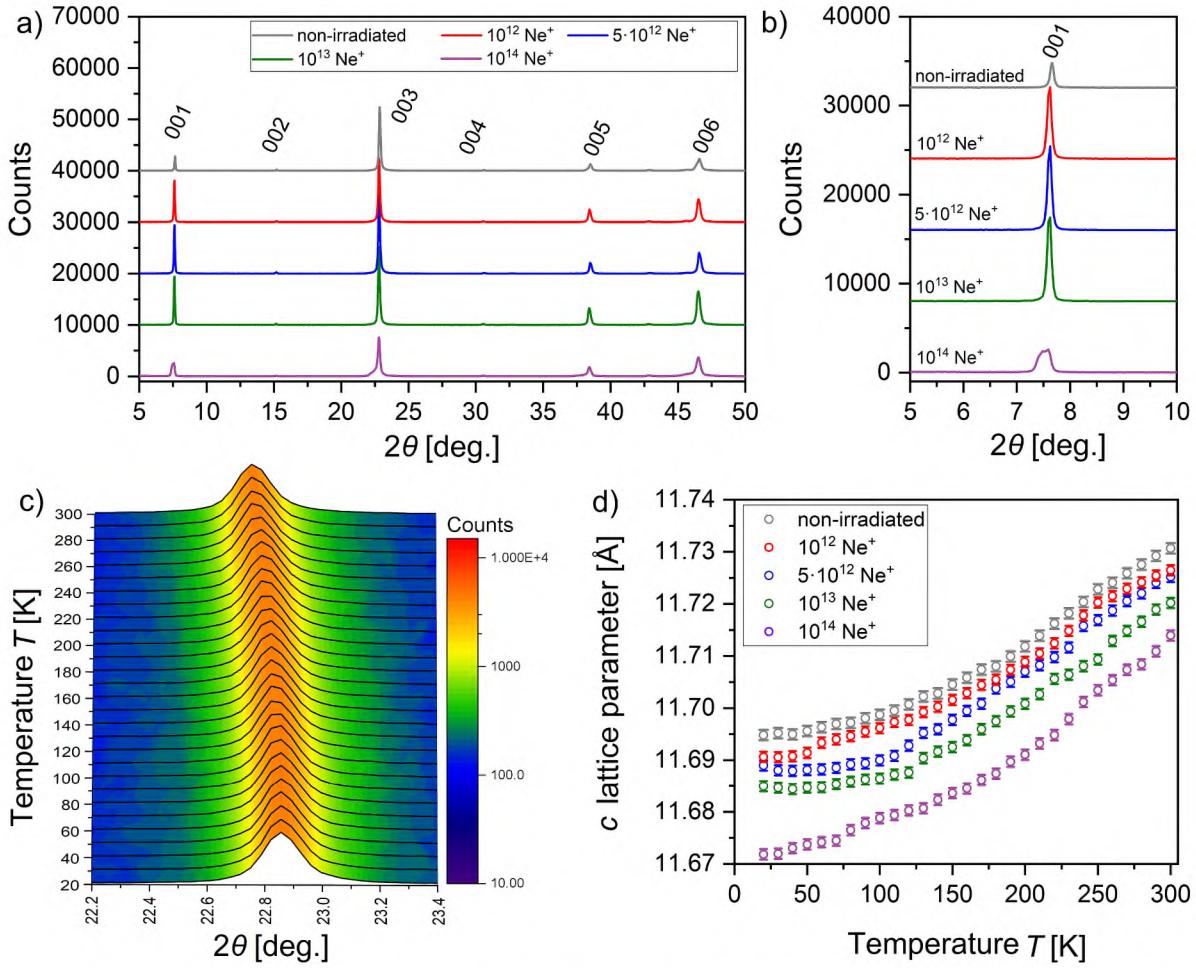

Fig. 4. The X-ray diffraction (XRD) studies of the non-irradiated and irradiated HTS tapes: (**a**) wide 2θ range patterns; (**b**) the magnification of the 001 reflections; (**c**) temperature dependence of the 003 reflection for the tape irradiated with the fluence of 10^{13} Ne^+/cm^2; (**d**) the *c* lattice parameter derived from the low temperature XRD studies.

studies were performed using the JEOL 5900 LV Scanning Electron Microscope (SEM). The structural properties of the samples modified by the Ne^+ ions were examined by Fourier-Transform infrared spectroscopy (FT-IR) and X-ray diffraction (XRD) methods. Phase homogeneity, defect formation, and the influence of the Ne^+ ions on the parameters of the orthorhombic superconducting phase were determined. Measurements of the samples by X-ray diffraction were performed using the Panalytical Empyrean powder diffractometer with a Cu-K_α radiation source. For low-temperature tests (15 – 300 K), the helium closed-circuit PheniX refrigerator by Oxford Instruments was used. The sample position was automatically corrected for thermal expansion. The obtained diffraction images were refined using the FullProf Rietveld software [58]. The Fourier Transform Infrared (FT-IR) spectra were collected using the Nicolet iS5 Thermo Scientific spectrometer equipped with the 1-reflection ATR diamond crystal and the DTGS detector. The spectra were collected in the range of 4000 – 500 cm^{-1}, with a 4 cm^{-1} spectral resolution.

The changes in T_c and J_c were detected by measurements of the AC magnetic susceptibility as a function of temperature and magnetic field of 0.44 Oe, magnetization as a function of the magnetic field strength, and the implantation dose. The magnetic measurements were conducted in zero field cooling (ZFC) mode using a standard inductance bridge operating at 189 Hz. The Stanford SR830 DSP lock-in amplifier acted as a signal voltmeter and a source of an AC current or AC magnetic field H_{AC}. The Lake Shore 330 temperature controller regulated the temperature with a chromelgold-iron thermocouple (accuracy of 0.3 K).

Resistance was measured by the four-point method as a function of temperature and the intensity of the external DC magnetic field H_{DC}. DC magnetic field was produced in a classic copper coil powered by the Glassman Europe Limited LV 20 – 50 DC power supply. The direction of the magnetic field was parallel to the longest side of the parallelepipedal sample and parallel to the current direction.

The DC magnetic measurements of the selected GdBCO tapes were performed using the Quantum Design superconducting quantum interference device magnetometer (SQUID, MPMS-5) in the 5 – 120 K temperature range, with a magnetic field of up to 50 kOe. The magnetic field was applied parallel to the *c*-axis of the crystal and to the *ab* (001) plane, which is perpendicular to the *c*-axis.

The X-ray absorption spectroscopy (XAS) analyzes electronic structure, local bonding environments, and oxidation states. The XAS spectra were collected at the PIRX (former PEEM/XAS) beamline [59] at the SOLARIS National Synchrotron Radiation Center in Kraków, Poland [60]. All the measurements were executed in ultra-high vacuum (UHV) in the surface-sensitive total electron yield (TEY) mode with an energy resolution 100 – 250 meV.

3. Result and discussion

3.1. Microstructural characterization

In Fig. 3, the surfaces of the superconducting Gd-123 layers of the investigated tapes are presented. The superconducting layer shows a

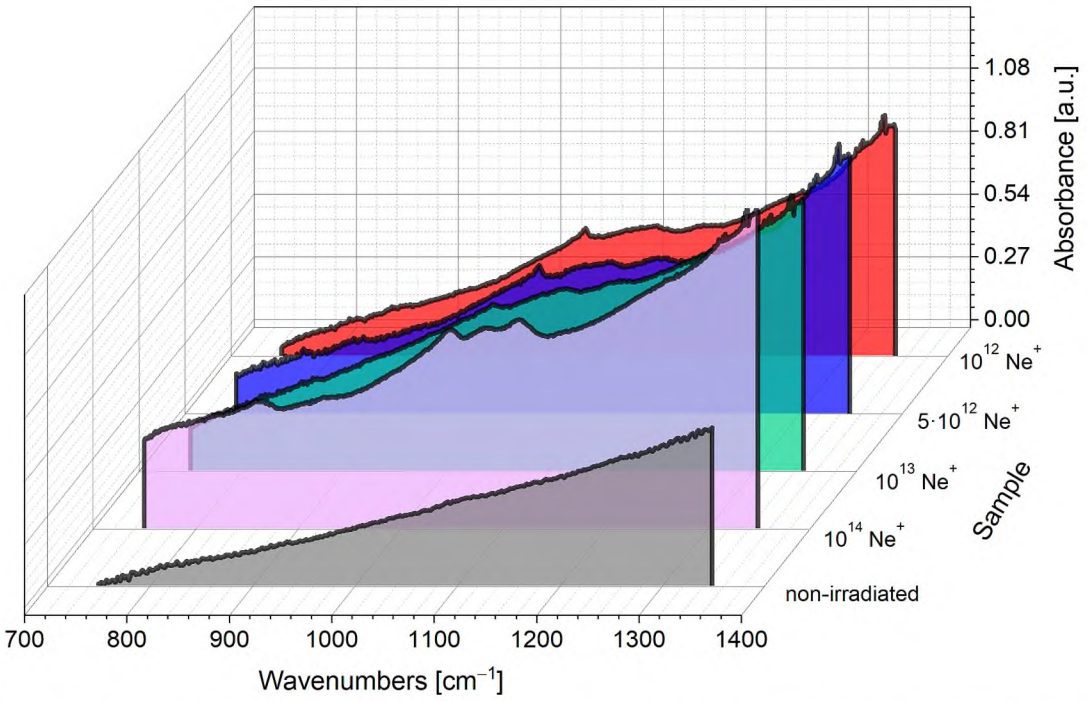

Fig. 5. The FT-IR spectra of the GdBCO layer of the 2G HTS tapes: non-irradiated, irradiated with the fluences: 10^{12}, $5{\cdot}10^{12}$, 10^{13}, and 10^{14} Ne^{+}/cm^{2} recorded at 298 K.

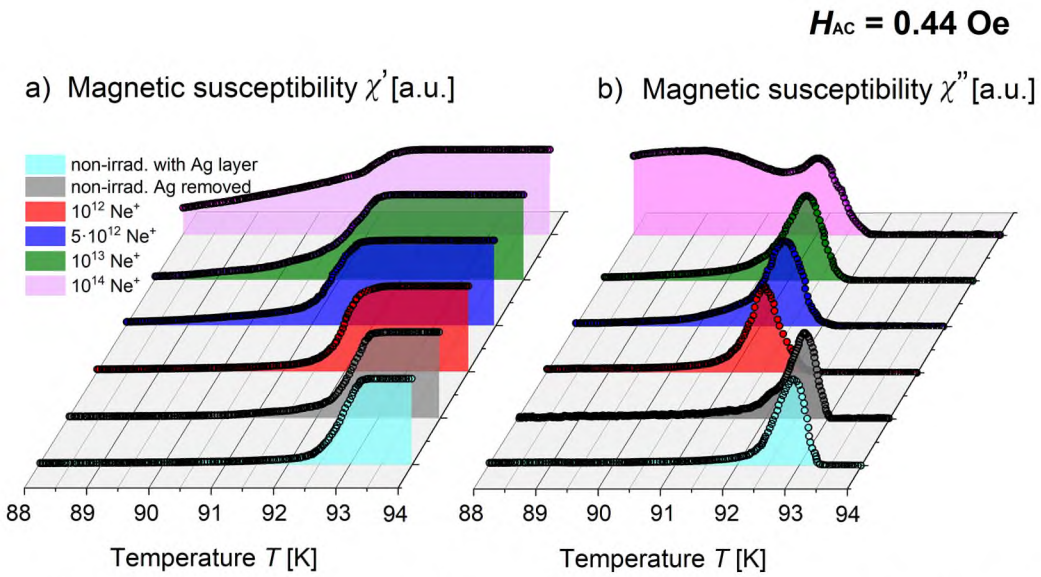

Fig. 6. Dispersion (**a**) and absorption (**b**) components of the normalized AC susceptibility as a function of temperature for the 2G HTS GdBCO tapes: before; after catalytical removal of the Ag protective layer; and after irradiation with the fluences of 10^{12}; $5{\cdot}10^{12}$; 10^{13}; 10^{14} Ne^{+}/cm^{2}.

porous microstructure with pores of about 1 – 4 μm in diameter. According to the EDS studies, the irregular structures visible in Fig. 3a and Fig. 3c are the residual Ag from the coating. Interestingly, the microstructures of the non-irradiated and moderately irradiated samples (up to $5{\cdot}10^{12}$ Ne^{+}/cm^{2}) are similar. The EDS maps presented in Fig. 3b-j for the latter tape show: the traces of remains of the Ag protective layer, Ni from the Hastelloy substrate (visible in pores of the HTS layer), and Ba originating from the GdBCO.

For the fluence of 10^{13} Ne^{+}/cm^{2}, the superconducting layer exhibits exfoliation, covering the pores with the partially loose HTS material (Fig. 3d). For the heavily irradiated tape (10^{14} Ne^{+}/cm^{2}), the exfoliated HTS material forms bubbles on the surface with a uniform diameter of about 1 μm (Fig. 3e-f). According to the EDS studies, small bright spots visible in the Fig. 3f are the Ag precipitations. The results revealed that heavy irradiation can introduce significant modifications to the microstructure of the superconducting layer.

3.2. *Structural characterization (XRD)*

The X-ray diffraction (XRD) studies revealed that the superconducting layers are grown with a high degree of texture. The Gd-123 structure of the bulk or film is orthorhombic (*Pmmm* symmetry). Only Bragg reflections of the 00l type were observed for the investigated tapes, as depicted in Fig. 4a-b. This is a sign that the [00l] direction is

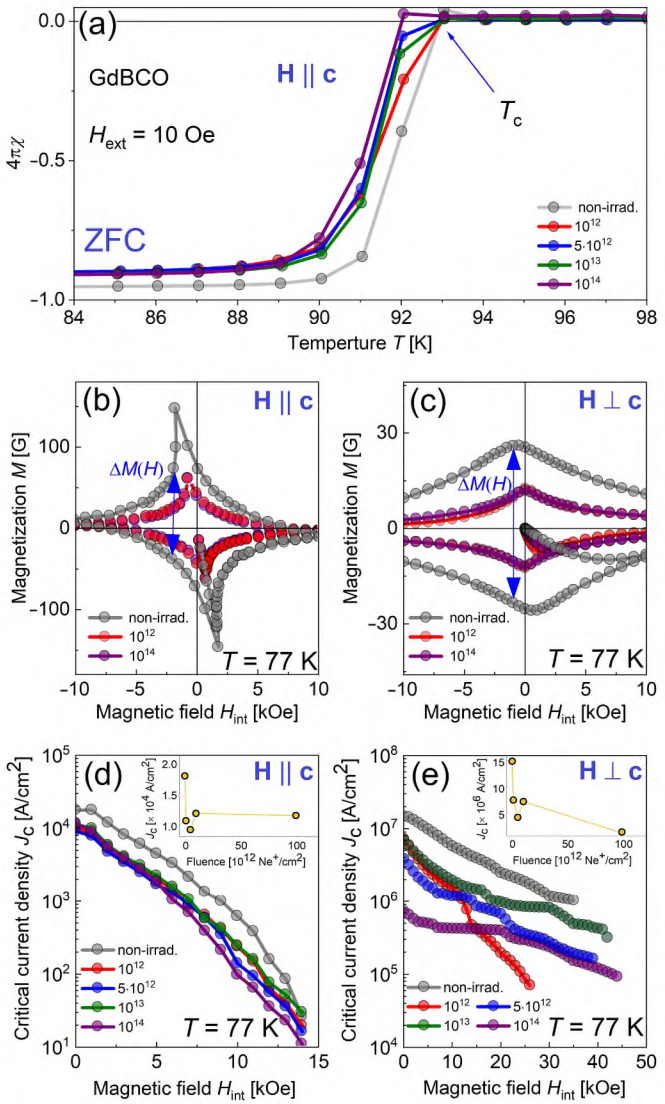

Fig. 7. The DC magnetic susceptibility vs. temperature for the field (**H || c**) of 10 Oe (**a**); Hysteresis loops recorded at 77 K for **H || c** (**b**) and **H ⊥ c** (**c**); Critical current density (J_c) as a function of magnetic field (Hint) in semilogarithmic scale for **H || c** (**d**) and **H ⊥ c** (**e**). Insets show critical current density vs. fluence at $T = 77$ K and $H_{int} = 10$ kOe.

normal to the plane surface. The 001 reflection shape for the heavily irradiated sample (10^{14} Ne$^+$/cm^2) differs significantly from the others. It is much broader what can be attributed to significant strain related to structural disorder induced by irradiation. Moreover, a gradual rise of the 001 reflection intensity results in oxygen deficiency at the 2*q* Wyckhoff site.

The Rietveld analyses of the diffraction patterns (at room and low temperatures) derive the *c* lattice parameters. Fig. 4c presents the behavior of the 003 reflection at low temperatures. It is apparent that the reflection moves towards lower scattering angles (higher lattice parameters) starting from 120 K. This is an expected behavior, later confirmed by the Rietveld analyses, the results of which are presented in Fig. 4d.

Interestingly, the lattice parameter decreases with increased fluency, possibly associated with a reduced oxygen index. Such behavior was reported for the bulk samples [43]. Moreover, the temperature dependence of the *c* lattice parameter, which reflects the lattice dynamics (via the Debye temperature), is quite similar for all specimens except the tape irradiated with the fluence of 10^{14} Ne$^+$/cm^2. The mentioned tape shows a substantially different curve than that observed for the non-implanted sample. That is typical for softening the phonon frequencies (lowering the Debye temperature). This result is consistent with the above-mentioned oxygen deficiency leading to vacancies in the oxygen-occupied sites.

3.3. *Fourier-transform infrared spectroscopy (FT-IR) measurements*

The IR low-frequency region (1350 – 750 cm^{-1}) was examined to check if the structure of the sample differs after irradiation. It is shown in Fig. 5 that tape exposure to the Ne$^+$ ion beam changed the surface of the GdBCO layer. Initially, there were no visible bands on the spectrum of the non-irradiated sample in the 1350 – 750 cm^{-1} wavenumber range. However, the bands at 1050, 1085, 1163 and 1318 cm^{-1} correspond to the C–O stretching vibrations, and the bands at 1116 and 1340 cm^{-1} corresponding with the CuOH or C–O stretching vibrations can be seen in the spectra of the irradiated by Ne$^+$ samples [61]. Those new vibrations could be due to formation of the carbonates or hydroxides surface after the CO_2 or H_2O absorption.

The intensity of the 1163 cm^{-1} band decreases drastically in the sample spectrum, irradiated with 10^{14} Ne$^+$ ions. For this sample, a new band at 862 cm^{-1} associated with the BaO bonding vibration was also observed [62].

The presented results indicate degradation of the sample structure caused by exposure of the tape to the Ne$^+$ ion beam. Furthermore, structural changes become more significant with increased Ne$^+$ doses.

3.4. *Magnetic investigations*

The AC susceptibility as a function of temperature was measured by a standard mutual inductance bridge operating with a frequency of 189 Hz. The measurements were conducted with a H_{AC} amplitude of 0.44 Oe. The tapes were oriented perpendicular to the AC magnetic field. Both the dispersive and absorption components of the AC susceptibility measured at $H_{AC} = 0.44$ Oe are presented in Fig. 6.

The susceptibility curves indicate the excellent 2G HTS GdBCO tapes before the Ne$^+$ ions irradiation. Removing the cover from the sample surface slightly deteriorated its superconducting properties. A slight decrease of the critical temperature by 0.3 K is visible, while the absorption peak is still sharp. The absorption susceptibility peaks remain narrow for the moderate irradiated tapes (10^{12}; $5{\cdot}10^{12}$; 10^{13} Ne$^+$/cm^2), indicating that the tapes maintained a homogeneous character throughout their volume. However, their critical temperatures are lower by about 1 – 1.2 K, which suggests oxygen deficiency due to irradiation. The exposure of the tapes to the Ne$^+$ ion beam caused partial destruction of the intergrain junctions, which resulted in the widening of the absorption peaks. For the heavy irradiated tape of 10^{14} Ne$^+$/cm^2, an additional broad maximum in the absorption part of the susceptibility curve was evidenced. This may indicate further destruction of the intergranular junctions caused by the radiation with the Ne$^+$ ions.

Fig. 7 presents the results of the DC magnetic measurements of the selected tapes of GdBCO. The dimensions $a \times b \times c$ (in cm) of these tapes were the following: for the non-irradiated tape – 0.3170 × 0.2250 × 0.0065; for irradiated with the fluence 10^{12} Ne$^+$/cm^2 – 0.3340 × 0.2050 × 0.0065; for irradiated with the fluence $5{\cdot}10^{12}$ Ne$^+$/cm^2 – 0.3390 × 0.2660 × 0.0065; for irradiated with the fluence 10^{13} Ne$^+$/cm^2 – 0.3080 × 0.3100 × 0.0065; for irradiated with the fluence 10^{14} Ne$^+$/cm^2 – 0.3360 × 0.1630 × 0.0065. Based on the corrections for demagnetization, according to Ref. [63], the quantities such as magnetization and critical current density, were presented as a function of internal magnetic field (H_{int}) [63].

Fig. 7a shows the $M(T)$ dependence, measured using zero-field-cooling (ZFC) procedure, in the DC external field of 10 Oe, oriented parallel to the *c*-axis, for all the investigated samples. A strong diamagnetic response around 93 K is observed for all the analyzed (non-irradiated and irradiated) samples (Fig. 7a). A sharp transition from the normal to superconducting state noticed for all the investigated samples

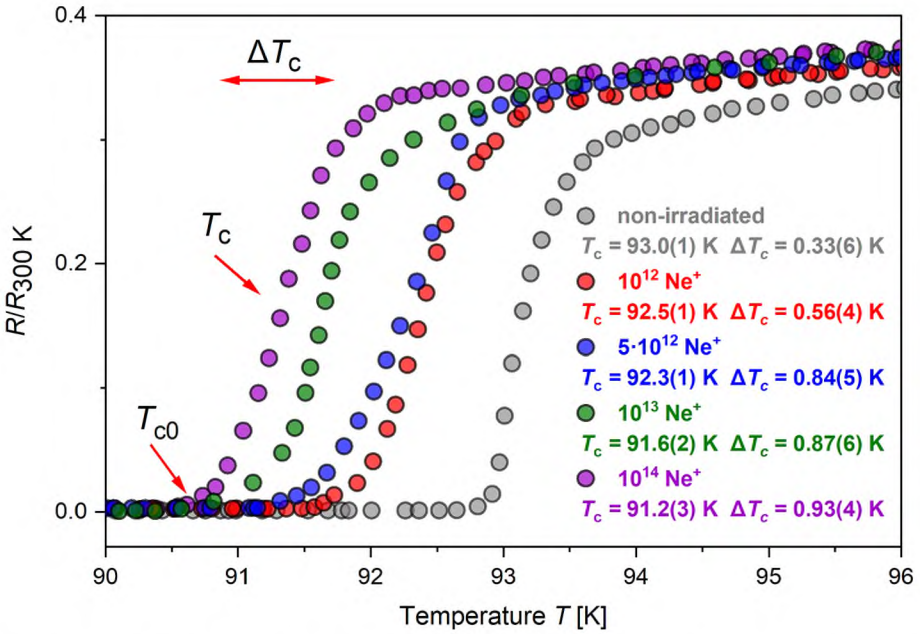

Fig. 8. The normalized resistivity ($R/R_{300\ K}$) as a function of temperature (T) near the superconducting transition.

with almost perfect Meissner effect confirms good quality of the tapes. Below T_c, one can observe slight degradation of the Meissner screening with increased Ne^+ fluence (Fig. 7a). A slight decrease of T_c can be observed for the tape subjected to the fluence of 10^{14} Ne^+/cm^2, compared to the reference sample and that subjected to the weaker Ne^+ fluence.

Fig. 7b shows the hysteresis loops of the studied samples, recorded at 77 K for the magnetic field oriented parallel to the *c*-axis. Using Bean's model for the rectangular shape sample, one can estimate the superconducting critical current density (J_c) [64–66]. In the case of **H** || **c**, we have $J_c^a = J_c^b = J_c^{ab}$, where current flows in the *ab* plane. The following formula was used to derive the critical current density J_c^{ab}:

$$J_c^{ab}(H) = \frac{20 \cdot \Delta M(H)}{a\left(1 - \frac{a}{3b}\right)} \quad (1)$$

Here, ΔM (in Gauss) is the width of the hysteresis loop (Fig. 7c), *a* and *b* are the sample dimensions (in cm) and the critical current density (J_c) is in $A \cdot cm^{-2}$. In the case of **H** || *ab* (**H** ⊥ **c**), when the current flows in the *cb* plane, we have $J_c^c = J_c^b = J_c^{cb}$. The following formula was used to derive the critical current density J_c^{cb}:

$$J_c^{cb}(H) = \frac{20 \cdot \Delta M(H)}{c\left(1 - \frac{c}{3b}\right)} \quad (2)$$

The magnetic field dependences of the critical current density (J_c) for all the investigated tapes, in the magnetic field geometries **H** || **c** and **H** ⊥ **c**, calculated according to Equations (1) and (2), are presented in Fig. 7d and Fig. 7e, respectively. The values of J_c for **H** ⊥ **c** are by two orders of magnitude higher than that for **H** || **c** and agree with the data reported recently [29]. Furthermore, suppression of the estimated critical current density value for the irradiated tapes can be noted when compared to the reference one for both magnetic field geometries. This can be seen clearly for the particular case determined at 77 K for H_{int} = 10 kOe (the insets of Fig. 7d and Fig. 7e) for which a decrease of J_c by three times was noticed for the irradiated samples in comparison with the non-irradiated one.

3.5. Resistivity measurements

The resistivity measurements as a function of temperature let to determine the critical temperatures of the superconductive transitions [67–70]. T_{c0} was discriminated by observing the gradient of the potential between the measuring contacts lesser than $E = 10^{-6}$ $V \cdot cm^{-1}$. The evidenced T_{c0} values were: 92.7 K for the reference (non-irradiated) sample, 91.5, 91.1, 90.7, and 90.5 K for the tapes irradiated with the fluences of 10^{12}, $5 \cdot 10^{12}$, 10^{13} and 10^{14} Ne^+/cm^2, respectively.

The changes in the width of the superconducting transition ΔT_c were assumed to be proportional to the FWHM of the gaussian peak fitted to the first derivative of the resistivity, while the centre of that peak was taken as a measure of T_c. The corresponding values are presented in Fig. 8. Similarly to the T_{c0}, the T_c shows a decrease with the fluence of about 2 K only. However, the differences are much higher when analyzing the transition width. Therefore, a factor of 3 must be considered to describe differences between the reference and the highly irradiated (10^{14} Ne^+/cm^2) samples. This indicates introducing inhomogeneities into the superconducting layers of the 2G HTS tapes.

3.6. X-ray absorption spectroscopy

The XAS spectra for the investigated tapes are presented in Fig. 9. The changes after irradiation affect mostly the O *K*-edge. This is consistent with the XRD studies that revealed oxygen deficiency after irradiation. According to the Fig. 9a, the Zhang-Rice singlet (ZRS) at 529 eV and the upper Hubbard band (UHB) at 529.9 eV can be observed clearly for the non-irradiated sample. The ZRS is dominant over the UHB for the superconducting *RE*BCO materials [70]. Those contributions became smaller for irradiated samples, and their ratio also changed. The third contribution, associated with chain holes (CH), is distinguishable only for raw sample.

As apparent from Fig. 9a, the ZRS was not evidenced in heavily irradiated samples, which indicates deterioration of the superconducting properties. The spectrum regions of 532 – 535 eV originate from the hybridized Gd-5*d* and O-2*p* orbitals, with two apparent features arising from the oxygen deficiency in irradiated specimens. The strong Gd-5*d* – O-2*p* hybridization is reflected in Gd $M_{4,5}$-lines shift towards higher energies after the Ne^+ irradiation, as discussed later.

The Cu $L_{2,3}$-edges (Fig. 9b) look similar, but for raw tape and one irradiated with a fluence of 10^{12} Ne^+/cm^2, screening effects can be noticed as the $2p^63d^{10}L$ contribution. This contribution originates from the so-called ligand hole and indicates the charge movement along the Cu–O chains and Cu–O_2 planes, which is proportional to observed O *K*-

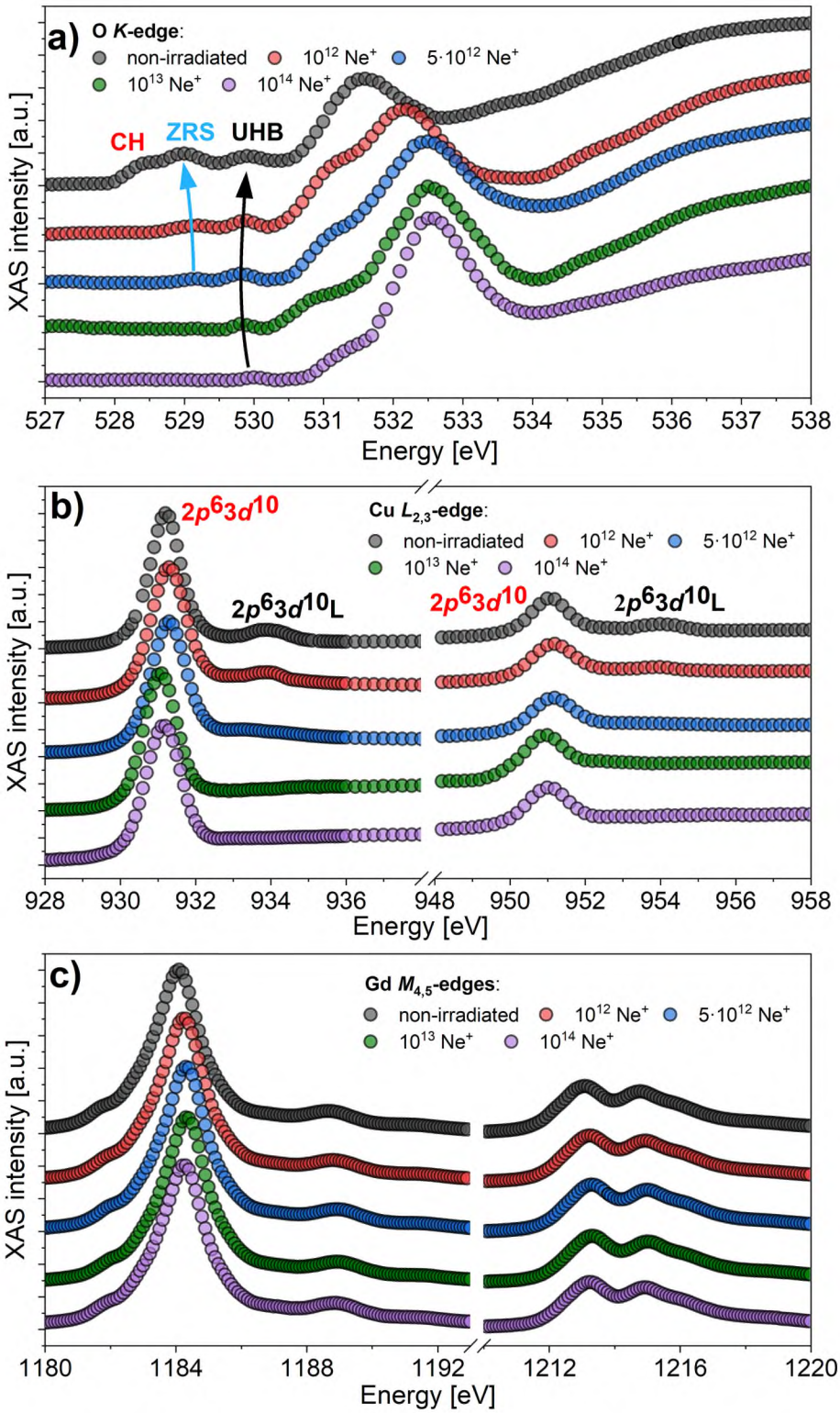

Fig. 9. The X-ray absorption spectra (XAS) for the GdBCO 2G HTS tapes: O *K*-edge (**a**); Cu $L_{2,3}$-edges (**b**); Gd $M_{4,5}$-edges (**c**). CH – chain holes; ZRS – Zhang-Rice singlet; UHB – Upper Hubbard band.

edge (ZRS) screening effects.

For the Gd $M_{4,5}$-edges, all the samples exhibit the spectra typical of the trivalent configuration of the Gd^{3+} ion (Fig. 9c). This proves that irradiation does not change the Gd valence. However, the spectrum for the non-irradiated sample is apparently shifted towards lower energies than the irradiated samples. This indicates that the Gd states also reflect oxygen depletion due to irradiation.

The limited penetration depth of soft X-rays, giving the information only from several nm, allows to observe the signal just from the surface of the sample, which was most affected by ions bombardment. Therefore, the results cannot be considered as meaningful for the entire bulk of the tape. However, the proposed mechanism of deterioration superconducting properties is entirely supported by XAS measurements.

4. Conclusions

Irradiation with high energy ions, simulating severe radiation damage, is significant for possible usage of the 2G HTS tapes for demanding applications in the space industry or nuclear applications (accelerators, reactors, etc.), The XRD and XAS results point to oxygen deficiency in the irradiated samples. Mainly, altering changes in the 001 reflection intensity together with a decrease of the *c* lattice parameter, the disappearance of the ZHR and UHB in the O *K*-edge as well as the $2p^6 3d^{10}\underline{L}$ in the Cu $L_{2,3}$-edges are proof of this mechanism. According to our results, the mechanism of the HTS tape deterioration is related to introducing oxygen vacancies rather than changing the microstructure of the HTS layer for the lower fluences (up to 10^{13} Ne^{+}/cm^{2}). The HTS layer starts to exfoliate for the highest doses; hence, the degradation mechanism is of microstructural origins. In the absence of a magnetic field, the decrease of critical current densities of about 33% was noticed when compared to the reference tape, while that reduction reaches 60% (at 10 kOe) for higher magnetic fields. Despite heavy damage caused by the highest fluence to the surfaces of HTS layers, the tape still preserves decent properties in bulk.

CRediT authorship contribution statement

Paweł Pęczkowski: Conceptualization, Methodology, Validation, Formal analysis, Investigation, Resources, Writing – original draft, Writing – review & editing, Visualization, Data curation, Project administration. **Ryszard Zalecki:** Formal analysis, Investigation, Writing – review & editing, Visualization, Data curation. **Piotr Zachariasz:** Validation, Investigation, Writing – review & editing. **Elżbieta Szostak:** Validation, Formal analysis, Investigation, Writing – review & editing, Visualization, Data curation. **Jarosław Piętosa:** Validation, Formal analysis, Writing – review & editing, Data curation. **Marcin Turek:** Resources, Writing – review & editing. **Krzysztof Pyszniak:** Resources. **Marcin Zając:** Supervision. **Joanna Czub:** Investigation, Writing – review & editing. **Łukasz Gondek:** Validation, Investigation, Resources, Writing – original draft, Writing – review & editing, Visualization, Supervision.

Declaration of Competing Interest

The authors declare that they have no known competing financial interests or personal relationships that could have appeared to influence the work reported in this paper.

Data availability

Data will be made available on request.

Acknowledgments

The authors would like to express their deepest gratitude to Dr. Joanna Stępień from the Academic Centre for Materials and Nanotechnology AGH, the PIRX beamline operator at the SOLARIS National Synchrotron Radiation Center at the Jagiellonian University, Dr. Andrzej Droździel from the Institute of Physics the University of Maria Curie-Skłodowska, for assisting during irradiation of the samples, and Dr. Sławomir Prucnal from the Helmholtz-Zentrum Dresden-Rossendorf (HZDR) for valuable and interesting discussions.

References

[1] M.V. Selvmanickam, High-temperature superconductor (HTS) wires and tapes, [in:] High-temperature superconductors (HTS) for energy applications, in: Z. Melhem (Ed.), High-temperature superconductors (HTS) for energy applications, Woodhead Publishing, Oxford, UK, 2011.

[2] J.G. Bednorz, K.A. Müller, Possible high T_c superconductivity in the Ba–La–Cu–O system, Z. Phys. B 64 (1986) 189–193, https://doi.org/10.1007/BF01303701.

[3] T.H. Geballe, J.K. Hulm, Superconductors in electronic-power technology, Sci. Am. 243 (5) (1980) 138–172, https://doi.org/10.1038/scientificamerican1180-138.

[4] C.W. Chu, P.H. Hor, R.L. Meng, I. Gao, Z.J. Huang, Y.Q. Wang, Evidence for superconductivity above 40 K in the La–Ba–Cu–O compound system, Phys. Rev. Lett. 58 (1987) 405–407, https://doi.org/10.1103/PhysRevLett.58.405.

[5] M.K. Wu, J.R. Ashburn, C.J. Torng, P.H. Hor, R.L. Meng, L. Gao, Z.J. Huang, Y. Q. Wang, C.W. Chu, Superconductivity at 93 K in a new mixed-phase Y–Ba–Cu–O compound system at ambient pressure, Phys. Rev. Lett. 58 (1987) 908–910, https://doi.org/10.1103/PhysRevLett.58.908.

[6] H.C. Yang, M.H. Hsieh, H.H. Sung, C.H. Chen, H.E. Horng, Y.S. Kan, H.C. Chen, J. C. Jao, High-temperature resistivity of $RBa_2Cu_3O_{7-x}$, where R = La, Pr, Nd, Sm, Eu, Dy, Ho, Er and Tm, Phys. Rev. B 39 (1989) 9203–9208, https://doi.org/10.1103/PhysRevB.39.9203.

[7] S.J. Jin, R.A. Fastnacht, T.H. Tiefel, R.C. Sherwood, Transport critical current in rare-earth-substituted superconductors $RBa_2Cu_3O_{7-\delta}$ (R = Gd, Dy, Sm, Ho, Y), Phys. Rev. B 37 (1988) 5828–5830, https://doi.org/10.1103/PhysRevB.37.5828.

[8] P. Pęczkowski, M. Kowalik, P. Zachariasz, C. Jastrzębski, Z. Jaegermann, P. Szterner, W.M. Woch, J. Szczytko, Synthesis and physicochemical properties of Nd-, Sm-, Eu-based cuprate high-temperature superconductors, Phys. Stat. Soli. A 215 (2018) 1700888, https://doi.org/10.1002/pssa.201700888.

[9] V. Dombrovski, D. Driscoll, B.A. Shoykhet, S.D. Umans, J.K. Zevchek, Design and testing of a 1000-hp high-temperature superconducting motor, IEEE Trans. Energy Conv. 20 (3) (2005) 638–643, https://doi.org/10.1109/TEC.2005.847946.

[10] Y.K. Kwon, M.H. Sohn, S.K. Baik, E.Y. Lee, J.M. Kim, T.S. Moon, H.J. Park, Y. C. Kim, K.S. Ryu, Development of a 100 hp synchronous motor with HTS field coils, IEEE Trans. Appl. Superconduc. 15 (2005) 2194–2197, https://doi.org/10.1109/TASC.2005.849610.

[11] V.M.R. Zermeno, A.B. Abrahamsen, N. Mijatovic, M.P. Sorensen, B.B. Jensen, N. F. Pedersen, Simulation of an HTS synchronous superconducting generator, Phys. Procedia 36 (2012) 786–790, https://doi.org/10.1016/j.phpro.2012.06.043.

[12] K. Sivasubramaniam, T. Zhang, M. Lokhandwalla, E.T. Laskaris, J.W. Bray, B. Gerstler, M.R. Shah, J.P. Alexander, Development of a high speed HTS generator for airborne applications, IEEE Trans. Appl. Superconduc. 19 (2009) 1656–1661, https://doi.org/10.1109/TASC.2009.2017758.

[13] P.N. Barnes, M.D. Sumption, G.L. Rhoads, Review of high power density superconducting generators: present state and prospects for incorporating YBCO windings, Cryogenics 45 (2005) 670–686, https://doi.org/10.1016/j.cryogenics.2005.09.001.

[14] T. Janowski, B.A. Głowacki, G. Wojtasiewicz, S. Kozak, J. Kozak, B. Kondratowicz-Kucewicz, M. Majka, M. Woźniak, Fault current limitation in power network by the superconducting transformer made of 2G HTS, IEEE Trans. Appl. Supercond. 21 (3) (2011) 1413–1416, https://doi.org/10.1109/TASC.2011.2112325.

[15] V.S. Vysotsky, S.S. Fetisov, V.V. Zubko, S.Y. Zanegin, A. Nosov, S.M. Ryabov, N. Bykovskiy, G.G. Svalov, E.P. Volkov, L.S. Fleishman, E.A. Dzhafarov, Development and test results of HTS windings for superconducting transformer with 1 MVA rated power, IEEE Trans. Appl. Supercond. 27 (4) (2016) 1–5, https://doi.org/10.1109/TASC.2016.2639011.

[16] S. Mukoyama, M. Yagi, N. Hirano, N. Amemiya, N. Kashima, S. Nagaya, T. Izumi, Y. Shiohara, Study of an YBCO HTS transmission cable system, Phys. C: Supercond. 463 (2003) 1150–1153, https://doi.org/10.1016/j.physc.2007.03.452.

[17] R. Wesche, A. Anghel, B. Jakob, G. Pasztor, R. Schindler, G. Vécsey, Design of superconducting power cables, Cryogenics 39 (1999) 767–775, https://doi.org/10.1016/S0011-2275(99)00098-3.

[18] H.W. Weijers, U.P. Trociewitz, W.D. Markiewicz, J. Jiang, D. Myers, E. E. Hellstrom, A. Xu, J. Jaroszyński, P. Noyes, Y. Viouchkov, D.C. Larbalestier, High field magnets with HTS conductors, IEEE Trans. Appl. Supercond. 20 (3) (2010) 576–582, https://doi.org/10.1109/TASC.2010.2043080.

[19] I. Rudnev, D. Abin, S. Pokrovskii, I. Anishchenko, A. Starikovskii, M. Osipov, T. Kulevoy, P. Fedin, K. Pryanishnikov, R. Batulin, A. Kiiamov, Influence of ion irradiation on critical characteristics of second-generation HTSC tapes, IEEE Trans. Appl. Supercond. 32 (4) (2022) 8000905, https://doi.org/10.1109/TASC.2022.3164629.

[20] K. Wang, H. Dong, D. Huang, H. Shang, B. Xie, Q. Zou, L. Zhang, C. Feng, H. Gu, F. Ding, Advances in second-generation high-temperature superconducting tapes and their applications in high-field magnets, Soft Sci. 2 (12) (2022) 1–28, https://doi.org/10.20517/ss.2022.10.

[21] R. Kwoka, J. Kozak, M. Majka, Test of HTS 2G superconducting tapes using the labview environment, App. Comp. Sci. 14 (1) (2018) 64–72, https://doi.org/10.23743/acs-2018-06.

[22] P. Spillantini, Superconducting magnets and mission strategies for protection from ionizing radiation in interplanetary manned missions and interplanetary habitats, Acta Astronaut. 68 (9–10) (2011) 1430–1439, https://doi.org/10.1016/j.actaastro.2010.07.023.

[23] S. Agostinelli, J. Allison, K. Amako, J. Apostolakis, H. Araujo, P. Arce, M. Asai, D. Axen, S. Banerjee, G. Brrand, F. Behner, L. Bellagamba, J. Boudreau, L. Broglia, A. Brunengo, H. Burkhardt, S. Chauvie, J. Chuma, R. Chytracek, G. Cooperman, G. Cosmo, P. Degtyarenko, A. Dell'Acqua, G. Depaola, D. Dietrich, R. Enami, A. Feliciello, C. Ferguson, H. Fesefeldt, G. Folger, F. Foppiano, A. Forti, S. Garelli, S. Giani, R. Giannitrapani, D. Gibin, J.J. Gómez Cadenas, J. González, G. Gracia Abril, G. Greeniaus, W. Greiner, V. Grichine, A. Grossheim, S. Guatelli, R. Gumplinger, R. Hamatsu, K. Hashimoto, H. Hasui, A. Heikkinen, A. Howard, V. Ivanchenko, A. Johnson, F.W. Jones, J. Kallenbach, N. Kanaya, M. Kawabata, Y. Kawabata, M. Kawaguti, S. Kelner, P. Kent, A. Kimura, T. Kodama, R. Kokoulin, M. Kossov, H. Kurashige, E. Lamanna, T. Lampén, V. Lara, V. Lefebure, F. Lei, M. Liendl, W. Lockman, F. Longo, S. Magni, M. Maire, E. Medernach, K. Minamimoto, P. Mora de Freitas, Y. Morita, K. Murakami, M. Nagamatu, R. Nartallo, P. Nieminen, T.

Nishimura, K. Ohtsubo, M. Okamura, S. O'Neale, Y. Oohata, K. Paech, J. Perl, A. Pfeiffer, M.G. Pia, F. Ranjard, A. Rybin, S. Sadilov, E. Di Salvo, G. Santin, T. Sasaki, N. Savvas, Y. Sawada, S. Scherer, S. Sei, V. Siritenko, D. Smith, N. Starkov, H. Stoecker, J. Sulkimo, M. Takahata, S. Tanaka, E. Tcherniaev, E. Safai Tehrani, M. Tropeano, P. Truscott, H. Uno, L. Urban, P. Urban, M. Verderi, A. Walkden, W. wander, H. Weber, J.P. Wellisch, T. Wenaus, D.C. Williams, D. Wright, T. Yamada, H. Yoshida, D. Zschiesche, GEANT4 – a simulation toolkit, Nucl. Instrum. Meth. Phys. Res. Sec. A: Accelerators, Spectrometers, Detectors and Associated Equipment A 506 (3) (2003) 250–303, doi:1016/S0168-9002(03)01368-8.

[24] A. Fassò, A. Ferrari, J. Ranft, P.R. Sala, FLUKA: present status and future developments, in: A. Menizone, A. Scribano (Eds.), Calorimetry in High Energy Physics, World Sci, Singapure, 1994, pp. 493–502.

[25] S.A. Washburn, S.R. Blatting, R.C. Singleterry, S.C. Westover, Analytical-HZETRN model for rapid assessment of active magnetic radiation shielding, Adv. Space Res. 53 (2014) 8–17, https://doi.org/10.1016/j.asr.2013.09.038.

[26] J.W. Wilson, M. Kim, W. Schimmerling, F.F. Badavi, S.A. Thibeault, F.A. Cucinotta, J.L. Shinn, R. Kiefer, Issues in space radiation protection: galactic cosmic rays, Health Phys. 68 (1995) 50–58, https://doi.org/10.1097/00004032-199501000-00006.

[27] J.C. Chancellor, G.B.I. Scott, J.P. Sutton, Space radiation: the number one risk to astronaut health beyond low earth orbit, Life 4 (2014) 491–510, https://doi.org/10.3390/life4030491.

[28] J. Emhofer, M. Eisterer, H.W. Weber, Stress dependence of the critical currents in neutron irradiated (RE)BCO coated conductors, Supercond. Sci. Technol. 26 (3) (2013), 035009, https://doi.org/10.1088/0953-2048/26/3/035009.

[29] M. Eisterer, R. Fuger, M. Chudy, F. Hengstberger, H.W. Weber, Neutron irradiation of coated conductors, Supercond. Sci. Technol. 23 (1) (2010), https://doi.org/10.1088/0953-2048/23/1/014009.

[30] R. Fuger, M. Eisterer, H.W. Weber, YBCO coated conductors for fusion magnets, IEEE Trans. Appl. Supercond. 19 (2009) 1532–1535, https://doi.org/10.1109/TASC.2009.2018236.

[31] L. Antonova, T. Demikhov, A. Troitskii, A. Didyk, A. Kobzev, A. Yurasov, S. Samoilenkov, G. Mikhailova, Effect of 2.5 MeV proton irradiation on the critical parameters of composite HTS tapes, Phys. Stat. Soli. C 12 (2015) 94–97, https://doi.org/10.1002/pssc.201400104.

[32] N. Haberkorn, J. Kim, S. Suárez, J.-H. Lee, S.-H. Moon, Influence of random point defects introduced by proton irradiation on the flux creep rates and magnetic field dependence of the critical current density J_c of co-evaporated $GdBa_2Cu_3O_{7-\delta}$ coated conductors, Supercond. Sci. Technol. 28 (2015), 125007, https://doi.org/10.1088/0953-2048/28/12/125007.

[33] L.M. Paulius, R.E. Shamu, S. Ferguson, M.C. Andrade, M.B. Maple, Effects of proton irradiation on the high-temperature superconducting system $Y_{1-x}Pr_xBa_2Cu_3O_{7-\delta}$, Appl. Phys. Lett. 71 (23) (1997) 3415–3417, https://doi.org/10.1063/1.120352.

[34] Z. Sefrioui, D. Arias, E.M. González, C. León, J. Santamaria, J.L. Vicent, Vortex liquid entanglement in irradiated $YBa_2Cu_3O_7$ thin films, Phys. Rev. B 63 (2001), 064503, https://doi.org/10.1103/PhysRevB.63.064503.

[35] M.A. Navacerrada, D. Arias, Z. Sefrioui, G. Loos, M.L. Lucía, J. Santamaría, F. Sánchez-Quesada, M. Varela, Critical temperature depression and persistent photoconductivity in ion irradiated $YBa_2Cu_3O_{7-x}$ films and $YBa_2Cu_3O_{7-x}$/$PrBa_2Cu_3O_7$ superlattices, Appl. Phys. Lett. 76 (22) (2000) 3289–3291, https://doi.org/10.1063/1.126609.

[36] R.J. Nicholls, S. Diaz-Moreno, W. Iliffe, Y. Linden, T. Mousavi, M. Aramini, M. Danaie, C.R.M. Grovenor, S.C. Speller, Understanding irradiation damage in high-temperature superconductors for fusion reactors using high resolution X-ray absorption spectroscopy, Commun. Mat. 3 (1) (2022) 52, https://doi.org/10.1038/s43246-022-00272-0.

[37] G.J. Clark, A.D. Marwick, R.H. Koch, R.B. Laibowitz, Effects of radiation damage in ion-implanted thin films of metal-oxide superconductors, App. Phys. Lett. 51 (1987) 139–141, https://doi.org/10.1063/1.98594.

[38] A. Glatz, I.A. Sadovskyy, U. Welp, W.-K. Kwok, G.W. Crabtree, The quest for high critical current in applied high-temperature superconductors, J. Superconduc. Nov. Mag. 33 (2020) 127–141, https://doi.org/10.1007/s10948-019-05255-w.

[39] A.V. Troitskii, T.E. Demikhov, L.K. Antonova, A.Y. Didik, G.N. Mikhailova, Radiation effects in high-temperature composite superconductors, J. Surf. Invest. X-ray, Synchrotron Neutron Tech. 10 (2016) 381–392, https://doi.org/10.1134/S1027451016020397.

[40] L. Antonova, A. Troitskii, G. Maikhailova, T. Demikhov, S. Kuzmichev, V. Skuratov, V. Semina, Changes in critical parameters of $GdBa_2Cu_3O_{7-x}$ HTS-2G due of swift-ion irradiation, Phys. Stat. Soli. B 256 (5) (2019) 1800255, https://doi.org/10.1002/pssb.201800255.

[41] A.V. Troitskii, L.K. Antonova, T.E. Demikhov, V.A. Skuratov, V.K. Semina, G. N. Mikhailova, The effect of Xe ion irradiation (40, 80 MeV) on HTS-2G $GdBa_2Cu_3O_{7-x}$, Phys. C: Supercond. Appl. 572 (2020) 1353631, https://doi.org/10.1016/j.physc.2020.1353631.

[42] E.I. Suvorova, P.N. Degtyarenko, I.A. Karateev, A.V. Ovcharov, A.L. Vasiliev, V. A. Skuratov, P.A. Buffat, Energy dependent structure of Xe ion tracks in YBCO and the effect on the superconductive properties in magnetic fields, J. Appl. Phys. 126 (2019), 145106, https://doi.org/10.1063/1.5120894.

[43] Y. Jia, M. LeRoux, D.J. Miller, J.G. Wen, W.-K. Kwok, U. Welp, M.W. Rupich, X. Li, S. Sathyamurthy, S. Flesher, A.P. Malozemoff, A. Kayani, O. Ayala-Valenzuela, L. Civale, Doubling the critical current density of high temperature superconducting coated conductors through proton irradiation, Appl. Phys. Lett. 103 (2013), 122601, https://doi.org/10.1063/1.4821440.

[44] L. Civale, A.D. Marwick, M.W.M. Elfresh, T.K. Worthington, A.P. Malozemoff, F. H. Holtzberg, J.R. Thompson, M.A. Kirk, Defect independence of the irreversibility line in proton-irradiated crystals Y-Ba-Cu-O, Phys. Rev. Lett. 65 (9) (1990) 1164–1167, https://doi.org/10.1103/PhysRevLett.65.1164.

[45] W.J. Choi, D. Ahmad, Y.I. Seo, R.K. Ko, Y.S. Kwon, Effect of the proton irradiation on the thermally activated flux flow in superconducting SmBCO coated conductors, Sci. Rep. 10 (2020) 2017, https://doi.org/10.1038/s41598-020-58936-1.

[46] M. LeRoux, K.J. Kihlstrom, S. Holleis, M.W. Rupich, S. Sathyamurthy, S. Fleshler, H.P. Sheng, D.J. Miller, S. Eley, L. Civale, A. Kayani, P.M. Niraula, U. Welp, W.-K. Kwok, Rapid doubling of the critical current of $YBa_2Cu_3O_{7-\delta}$ coated conductors for viable high-speed industrial processing, Appl. Phys. Lett. 107 (2015), 192601, https://doi.org/10.1063/1.4935335.

[47] M.W. Rupich, S. Sathyamurthy, S. Fleshler, Q. Li, V. Solovyov, T. Ozaki, U. Welp, W.-K. Kwok, M. LeRoux, D.J. Miller, K. Kihlstrom, L. Civale, S. Eley, A. Kayani, Engineered pinning landscapes for enhanced 2G coil wire, IEEE Trans. Appl. Supercond. 26 (2016) 6601904, https://doi.org/10.1109/TASC.2016.2542270.

[48] Y. Frenkel, Über die Wärmebewegung in festen und flüssigen Körpern (About the thermal motion in solids and liquids), Z. Phys. 35 (8–9) (1926) 652–669, https://doi.org/10.1007/BF01379812.

[49] P.H. Borcherds, C.E. Gough, W.F. Vinen, A.C. Warren, The Motion of Abrikosov vortices in a type II superconductor, Philosoph. Mag. 10 (104) (1964) 349–354, https://doi.org/10.1080/14786436408225674.

[50] J.F. Ziegler, M.D. Ziegler, J.P. Biersack, SRIM – The stopping and range of ions in matter (2010), Nuc. Instr. Meth. Phys. Res. B 268 (2010) 1818–1823, https://doi.org/10.1016/j.nimb.2010.02.091.

[51] J.P. Biersack, L.G. Haggmark, A Monte Carlo computer program for the transport of energetic ions in amorphous targets, Nuc. Instr. Meth. 174 (1–2) (1980) 257–269, https://doi.org/10.1016/0029-554X(80)90440-1.

[52] SuperPower Inc., SuperPower 2G-HTS wire specifications, https://www.superpower-inc.com/specification.aspx, 2023 (accessed 9 February, 2023).

[53] J. Jędryka, M. Szota, M. Nabiałek, A. Łukaszewicz, A. Bukowska, Studies of selected properties of high-temperature superconducting tape 2G HTS SF series - the example: tape SF12050, J. Achievem. Mat. Manufact. Eng. 61 (2) (2013) 187–194.

[54] M. Turek, S. Prucnal, A. Droździel, K. Pyszniak, Arc discharge ion source for europium and other refractory metals implantation, Rev. Sci. Instrum. 80 (2009), 043304, https://doi.org/10.1063/1.3117357.

[55] M. Turek, S. Prucnal, A. Droździel, K. Pyszniak, Versatile plasma ion source with an internal evaporator, Nuc. Instr. Meth. Phys. Res. Sec. B: Beam Interact. Mater. Atoms 269 (7) (2011) 700–707, https://doi.org/10.1016/j.nimb.2011.01.133.

[56] J.F. Ziegler, M.D. Ziegler, J.P. Biersack, The stopping and range of ions in mater, Nucl. Instr. Meth. B 268 (11–12) (2010) 1818–1823, https://doi.org/10.1016/j.nimb.2010.02.091.

[57] H. Gupta, K. Joshi, S.K. Gautam, R.G. Singh, F. Singh, Raman scattering from irradiated nanocrystalline zinc oxide thin films: Perspective view on effects of energy loss, ion fluence, and ion flux, Vacuum 181 (2020), 109598, https://doi.org/10.1016/j.vacuum.2020.109598.

[58] J. Rodriguez-Carvajal, Recent advances in magnetic structure determination by neutron powder diffraction, Physica B 192 (1993) 55–69, https://doi.org/10.1016/0921-4526(93)90108-I.

[59] M. Zając, T. Giela, K. Freindl, K. Kollbek, J. Korecki, E. Madej, K. Pitala, A. Kozioł-Rachwał, M. Sikora, N. Spiridis, J. Stępień, A. Szkudlarek, M. Ślęzak, T. Ślęzak, D. Wilgocka-Ślęzak, The first experimental results from the 04BM (PEEM/XAS) beamline at Solaris, Nuc. Instr. Meth. Phys. Res. B 492 (2021) 43–48, https://doi.org/10.1016/j.nimb.2020.12.024.

[60] J. Szlachetko, J. Szade, E. Beyer, W. Błachucki, P. Ciochoń, P. Dumas, K. Freindl, G. Gazdowicz, S. Glatt, K. Guła, J. Hormes, P. Indyka, A. Klonecka, J. Kołodziej, T. Kołodziej, J. Korecki, P. Korecki, F. Kosiorowski, K. Kosowska, G. Kowalski, M. Kozak, P. Kozioł, W. Kwiatek, D. Liberda, H. Lichtenberg, E. Madej, A. Mandziak, A. Marendziak, K. Matlak, A. Maximenko, P. Nita, N. Olszowska, R. Panaś, E. Partyka-Jankowska, M. Piszak, A. Prange, M. Rawski, M. Roman, M. Rosmus, M. Sikora, J. Sławek, T. Sobol, K. Sowa, N. Spiridis, J. Stępień, M. Szczepanik, T. Ślęzak, T. Tyliszczak, G. Ważny, J. Wiechecki, D. Wilgocka-Ślęzak, B. Wolanin, P. Wróbel, T. Wróbel, M. Zając, A. Wawrzyniak, M. Stankiewicz, SOLARIS National Synchrotron Radiation Centre in Krakow, Poland, Eur. Phys. J. Plus 138 (2023) 10, https://doi.org/10.1140/epjp/s13360-022-03592-9.

[61] S. Shinde, D. Dubal, G. Ghodake, P. Gómez-Romero, S. Kim, V. Fulari, Influence of Mn incorporation on the supercapacitive properties of hybrid CuO/$Cu(OH)_2$ electrodes, RSC Adv. 5 (39) (2015) 30478–30484, https://doi.org/10.1039/C5RA01093D.

[62] M.K. Trivedi, R.M. Tallapragada, A. Branton, D. Trivedi, O. Latiyal, S. Jana, Influence of biofield treatment on physical and structural characteristics of barium oxide and zinc sulfide, J. Laser. Opt. Photonics 2 (2) (2015) 1000122, https://doi.org/10.4172/2469-410X.1000122.

[63] R. Prozorov, V.G. Kogan, Effective demagnetizing factors of diamagnetic samples of various shapes, Phys. Rev. Appl. 10 (2018), 014030, https://doi.org/10.1103/PhysRevApplied.10.014030.

[64] C.P. Bean, Magnetization of hard superconductors, Phys. Rev. Lett. 8 (1962) 250–253, https://doi.org/10.1103/PhysRevLett.8.250.

[65] C.P. Bean, Magnetization of high-field superconductors, Rev. Mod. Phys. 36 (1964) 31–39, https://doi.org/10.1103/RevModPhys.36.31.

[66] E.M. Gyorgy, R.B. van Dover, K.A. Jackson, L.F. Schneemeyer, J.V. Waszczak, Anisotropic critical currents in $Ba_2YCu_3O_7$ analyzed using an extended Bean model, Appl. Phys. Lett. 55 (1989) 283–285, https://doi.org/10.1063/1.102387.

[67] P. Pęczkowski, P. Szterner, Z. Jaegermann, M. Kowalik, R. Zalecki, W.M. Woch, Effects of forming pressure on physicochemical properties of YBCO ceramics,

J. Superconduc. Nov. Mag. 31 (2018) 2719–2732, https://doi.org/10.1007/s10948-017-4513-7.

[68] P. Pęczkowski, P. Zachariasz, M. Kowalik, R. Zalecki, C. Jastrzębski, Characterization of the superconductor-multiferroic type materials based on $YBa_2Cu_3O_{7-\delta}$–$YMnO_3$, Cer. Int. 45 (15) (2019) 18189–18204, https://doi.org/10.1016/j.ceramint.2019.06.137.

[69] P. Pęczkowski, P. Zachariasz, M. Kowalik, W. Tokarz, S.P.K. Naik, J. Żukrowski, C. Jastrzębski, L.J. Dadiel, W. Tabiś, Ł. Gondek, Iron diffusivity into superconducting $YBa_2Cu_3O_{7-\delta}$ at oxygen-assisted sintering: structural, magnetic, and transport properties, J. Eur. Cer. Soc. 41 (14) (2021) 7085–7097, https://doi.org/10.1016/j.jeurceramsoc.2021.06.018.

[70] P. Pęczkowski, P. Zachariasz, C. Jastrzębski, J. Piętosa, E. Drzymała, Ł. Gondek, On the superconductivity suppression in $Eu_{1-x}Pr_xBa_2Cu_3O_{7-\delta}$, Materials 14 (13) (2021) 3503, https://doi.org/10.3390/ma14133503.